Electronic Supplementary Material (ESI) for Journal of Materials Chemistry A.

Supporting Information for

Atomically Co dispersed cross-channel hierarchical carbon-based electrocatalyst for high-performance oxygen reduction in Zn-Air battery

Liuhua Li[a], Xiangjian Liu[a], Jinming Wang[a], Rui Liu[a], Yarong Liu[a], Changli Wang[a], Wenxiu Yang [a], Xiao Feng[a], and Bo Wang[a]**

[a] Key Laboratory of Cluster Science Ministry of Education, Beijing Key Laboratory of Photoelectronic/Electrophotonic Conversion Materials, Advanced Technology Research Institute (Jinan), Advanced Research Institute of Multidisciplinary Science, School of Materials Science and Engineering, School of Chemistry and Chemical Engineering
Beijing Institute of Technology
No. 5, South Street, Zhongguancun, Haidian District, Beijing 100081, China
E-mail: yangwx19@bit.edu.cn and bowang@bit.edu.cn

Experimental methods

Materials. Gelatin (gel strength~250 g Bloom), Co $(NO_3)_2{\cdot}6H_2O$ (99%), 2-methylimidazole (2-mIM, AR), cetrimonium bromide (CTAB, AR), hydrofluoric acid (HF, 40-60%), potassium hydroxide (KOH, 85%) were obtained from Aladdin Co., Ltd. Tetraethoxysilane (99%) were purchased from Energy Chemical Co., Ltd. Zn $(NO_3)_2{\cdot}6H_2O$ (AR) and ethanol (EtOH, AR) were supplied by Beijing Chemical Reagent Company. The commercial 20 wt.% Pt/C catalyst were purchased from Shanghai Hesen Electric Co., Ltd. The commercial RuO_2 (99.95%) catalyst and Nafion solution (5 wt.%) were supplied by Alfa Aesar and InnoChem Co., Ltd, respectively. All chemicals were used without further purification.

Synthesis of SiO_2/CoZn-ZIF. First, SiO_2 nanospheres with an average diameter of 500 nm were synthesized as the templates through the Stöber method[1]. SiO_2 powder (0.5 g) and CTAB (0.5 g) was dispersed in water under stirring for 1 h, 5 mL water solution containing Zn $(NO_3)_2{\cdot}6H_2O$ (1.9833 g) and Co $(NO_3)_2{\cdot}6H_2O$ (0.2426 g) (molar ratio of Co and Zn is 1:8) was added under stirring for 1 h, followed by addition of 2.463g of 2-mIM. After continuously stirring for 4 h, the product (named as SiO_2/CoZn-ZIF) was collected by centrifugation and washed three times by ultrapure water, finally dried in oven at 60°C overnight.

Synthesis of CoSA@NPC. 0.5 g SiO_2/CoZn-ZIF and 0.25 g gelatin was dispersed in 5 mL water under stirring at 50 °C for 4 hours. The gelatinous product was freeze-dried for 12 hours at -50 °C, the obtained solid composites were thermally treated at 300 °C for 1 hour and 900 °C for 2 hours under nitrogen atmosphere (the heating rate is 5 °C/min). The pyrolyzed sample soaked in HF solution (20 wt.%) for 24 hours to remove unstable cobalt species. Finally, the acid-treated sample pyrolyzed by above pyrolysis process again to get CoSA@NPC.

Synthesis of NI-NPC, NS-NPC. The synthesis process of no ice template nitrogen-doped porous carbon catalyst (NI-NPC) and no silica template nitrogen-doped porous carbon catalyst (NS-NPC) is similar to CoSA@NPC, but the synthesis of NI-NPC without the freeze-drying process, moreover, the synthesis of NS-NPC without the addition of SiO_2 nanospheres.

Synthesis of Co@NPC-x. The synthesis process of Co@NPC-x (x=1, 5, 10, 15, x represents the molar ratio of Zn and Co) are same as CoSA@NPC, but change the molar ratio of Zn and Co.

Characterization. Powder X-ray diffraction (PXRD) patterns were recorded on a Rigaku MiniFlex600 Powder X-ray Diffractometer with a Cu Kα X-ray radiation source (λ = 0.154056 nm). Scanning electron microscopy (SEM) images were captured in JEOL model S-4800 scanning electron microscope operated at 5 kV voltage. TEM image was obtained on a HITACHI H-7700 transmission electron microscope at an accelerating voltage of 200 kV. The high-resolution transmission electron microscopy (HRTEM) images were collected on FEI Tecnai G2 F30 operating at 300 kV. The aberration-corrected high-angle annular dark-field scanning transmission electron microscopy (AC HAADF-STEM) images, energy-dispersive X-ray spectroscopy (EDX) were collected in Themis Z single spherical ACTEM operating at 300 kV. Raman spectroscopy was collected in Horiba Scientific LabRAM HR Evolution with 532 nm.

Nitrogen adsorption-desorption analysis was carried out on BELSORP-max II with nitrogen at 77 K. Brunauer–Emmett–Teller surface areas, pore size distributions were calculated based on the N_2 sorption isotherm using nonlocal density functional theory (NLDFT). All samples were activated at 120 °C for 12 h under vacuum before adsorption-desorption measurements.

Inductively coupled plasma optical emission spectroscopy (ICP-OES) was executed on Shimadzu ICPE-9800, and the samples were digested by HNO_3. X-ray photoelectron spectroscopy (XPS) was tested on PHI QUANTERA-II SXM with an Al Kα X-ray radiation source (0.68 eV). X-ray absorption fine structure (XAFS) spectroscopy was carried out at 1W2B end station, Beijing Synchrotron Radiation Facility (BSRF), and analysis was carried out on Athena software.

Electrochemical Characterization. All electrochemical measurements were performed using a rotating ring-disk electrode (RRDE, E7R9 model, Pine Research Instrumentation, USA). All catalysts were prepared by mixing 2 mg of the catalysts in 1 mL of solution (volume ratio of isopropanol, H_2O, and 5% Nafion solution is 100: 100: 1), followed by continuous ultrasonication to form homogeneous catalysts ink. Then, catalyst ink was loaded onto a rotation ring disk electrode (RRDE), as-prepared catalyst loading is 0.4 mg cm^{-2} and commercial 20 wt.% Pt/C electrocatalyst is 0.12 mg cm^{-2}. A three-electrode configuration with a rotating ring disk electrode (RRDE) was carried out to measure the electrocatalytic activity of catalysts. The glassy carbon (0.2475 cm^2), graphite rod and saturated calomel electrode (SCE) served as the working, counter and reference electrode, respectively. LSV was tested at 5 mV s^{-1} with 1600 rpm in 0.1 M KOH to evaluate ORR catalytic performance. The calibration of E_{SCE} to E_{RHE} was conducted in H_2-saturated electrolyte by applying cyclic voltammetry (CV) on a pair of Pt wires, which served as the working electrode and counter electrode, respectively. The average of potential at which the cathodic current and the anodic current both crossed zero was considered as thermodynamic potential for the hydrogen electrode reactions. And the function of E_{RHE} about E_{SCE} can be expressed as followed:

$$E_{RHE} = E_{SCE} + 0.9955\ \text{V} \qquad (1)$$

The kinetic current density (j_k) can be calculated by the Koutecky-Levich equation:

$$j_k = (j_L \times j)/(j_L - j). \qquad (2)$$

Where j is the measured current density, j_k is the kinetic current density, j_L is the obtained diffusion-limited current density.

The mass activity (j_m, mA cm^{-2}) of the prepared catalysts was calculated from the below equations:

$$j_m = j_k / (w_{Co} \times c_{catal}) \qquad (3)$$

Where c_{catal} is catalyst loading, w_{Co} (wt.%) is the weight percentage of Co sites determined by ICP-OES results.

Turnover frequency (TOF, e s^{-1} site^{-1}) of the prepared catalysts was calculated from the below equations:

$$\text{TOF} = j_k\ \text{Ne}\ M_{Co} / N_A\ w_{Co}\ c_{catal} \qquad (4)$$

where N_e is the electron number of per Coulomb (6.24 × 1018 e C^{-1}), M_{Co} is the molar mass of Co (58.933 g mol^{-1}), N_A is Avogadro constant (6.022×10^{23} mol^{-1}).

RRDE measurements were carried out to calculate the hydrogen peroxide yield (%H_2O_2) and the electron transfer number (n):

$$H_2O_2\% = 200 \times (i_r / N) / (i_d + i_r / N); \qquad (5)$$

$$n = 4 \times i_d / (i_d + i_r / N) \qquad (6)$$

where i_d and i_r are the disk and ring currents, respectively. N is determined to be 0.37.

Electrical double layer capacitance (C_{dl}) was estimated from the CV method at various scan rates (ν = 2, 5, 10, 20, 30, 40, 50 mV s^{-1}) in the non-Faradaic regions, and C_{dl} was given in the following equation:

$$\Delta j = j_{\mathrm{anodic}} - j_{\mathrm{cathodic}} = 2 \times v \times C_{\mathrm{dl}} \qquad (7)$$

Where Δj (mA cm^{-2}) is the measured capacitive current density at 1.12 V *vs*. RHE.

The electrochemical impedance spectroscopy (EIS) tests were carried out at 0.8 V vs RHE. The spectra were recorded in a frequency range from 0.01 to 10^5 Hz with a voltage amplitude of 5.0 mV.

Zn-Air battery tests. The home-made Zn-air battery was assembled. The as-prepared CoSA@NPC catalysts or 20% wt.% Pt/C were coated on the gas diffusion (GDL) layer as the air cathodes of Zn-air battery, and the catalyst mass loading of CoSA@NPC and 20% wt.% Pt/C is 2.0 mg cm^{-2} and 1.0 mg cm^{-2}, respectively. A polished Zn foil and 6 M KOH + 0.2 M Zn $(Ac)_2$ mixture solution was employed as the anode and electrolyte, respectively. For the charge-discharge cycling stability test, the CoSA@NPC or 20% wt.% Pt/C were mixed with commercial RuO_2 (mass ratio is 1:1) and then assembled into ZABs for test.

DFT calculation. The reaction energy profiles of ORR were investigated on CoN_4 by the Vienna Ab-initio Simulation Package (VASP) with the revised Perdew-Burke-Ernzerhof (RPBE) of the generalized gradient approximation (GGA). PAW pseudo-potential was adopted in the description of the interaction between ionic and valence electrons. The 5 × 5 supercell was used to simulate carbon layer. The defect in carbon was built by removing partial carbon atoms. The cutoff energy of 400 eV and energy convergence of 1×10^{-4} eV were used in all geometry optimization calculations. After geometry optimization, the charge density difference mappings and projected density of state (PDOS) were calculated with Monkhorst-Pack k-point mesh of 2 × 2 × 1, the cutoff energy of 400 eV and energy convergence of 1×10^{-4} eV. The reported standard hydrogen electrode (SHE) model was adopted in the calculations of Gibbs free energy changes (ΔG) of all reaction steps, which was used to evaluate the reaction barrier [2].

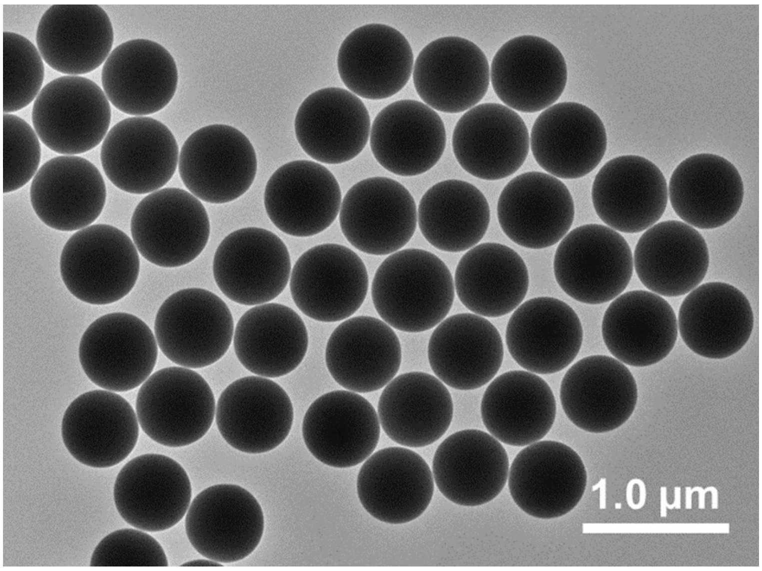

Fig. S1 TEM image of SiO_2 template.

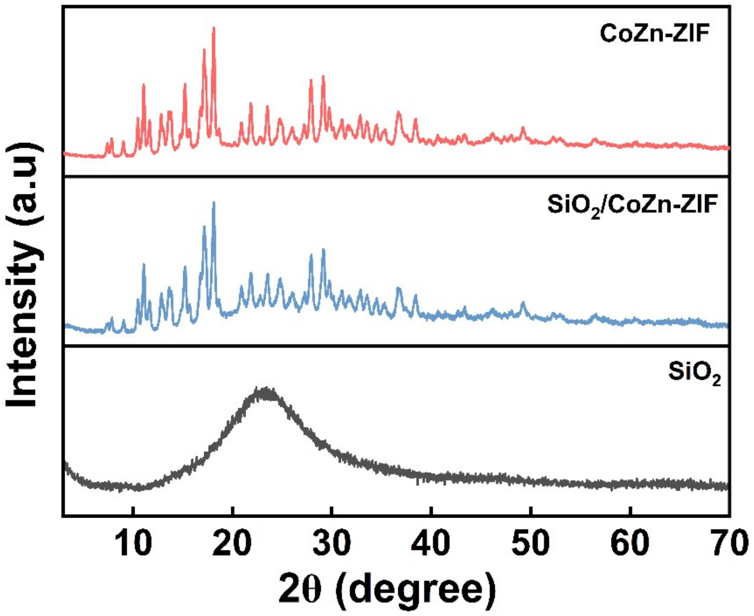

Fig. S2 XRD patterns of pure CoZn-ZIF, SiO_2/CoZn-ZIF and SiO_2.

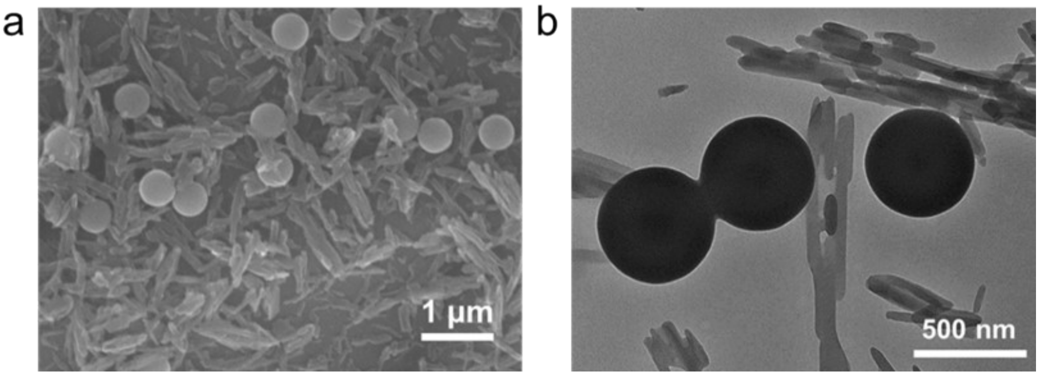

Fig. S3 (a) SEM and (b) TEM images of SiO_2/CoZn-ZIF.

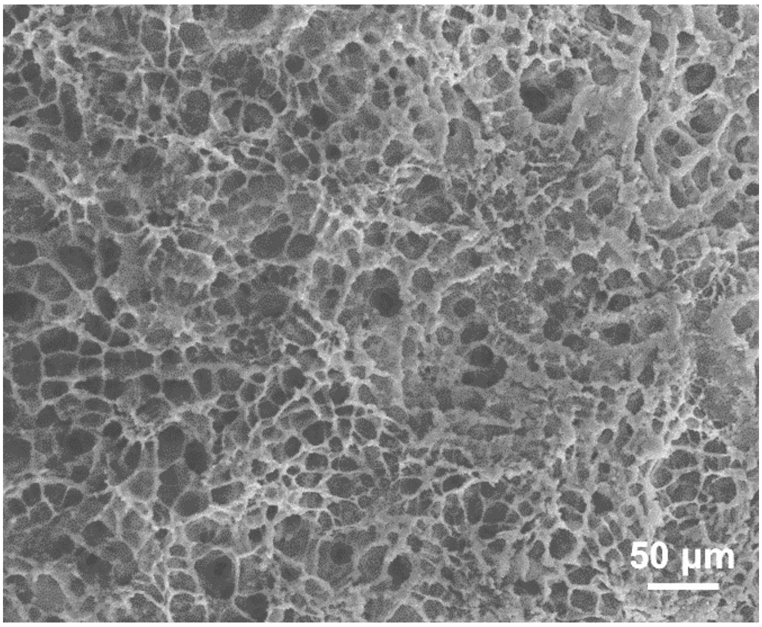

Fig. S4 SEM image of SiO_2/CoZn-ZIF/gelatin.

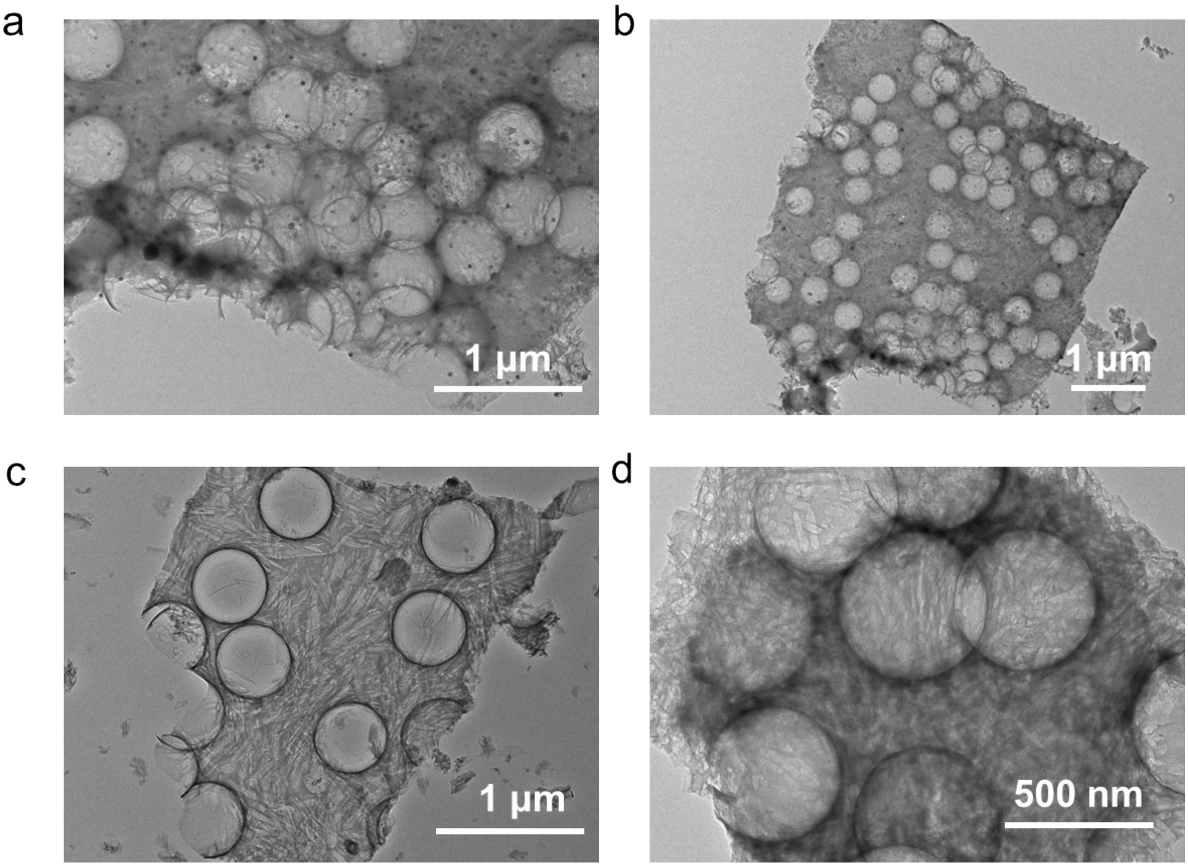

Fig. S5 The TEM images of (a) Co@NPC-1, (b) Co@NPC-5, (c) Co@NPC-10, (d) Co@NPC-15.

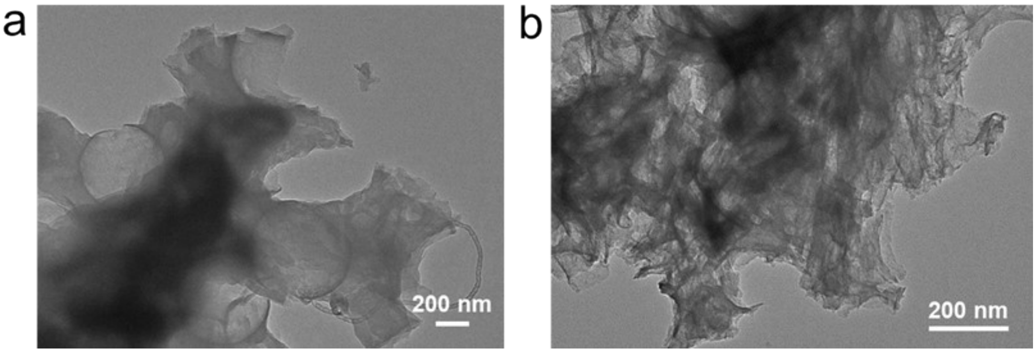

Fig. S6 TEM images of (a) NI-NPC and (b) NS-NPC.

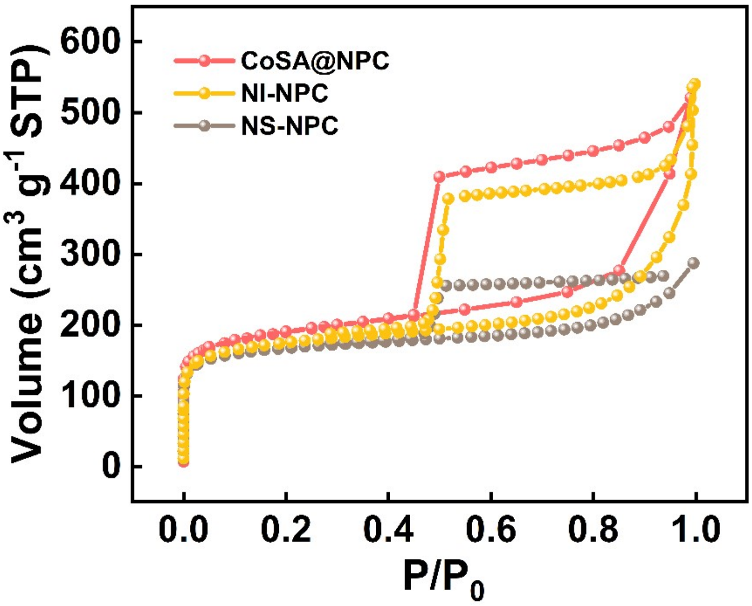

Fig. S7 Nitrogen adsorption/desorption isotherms of CoSA@NPC, NI-NPC and NS-NPC.

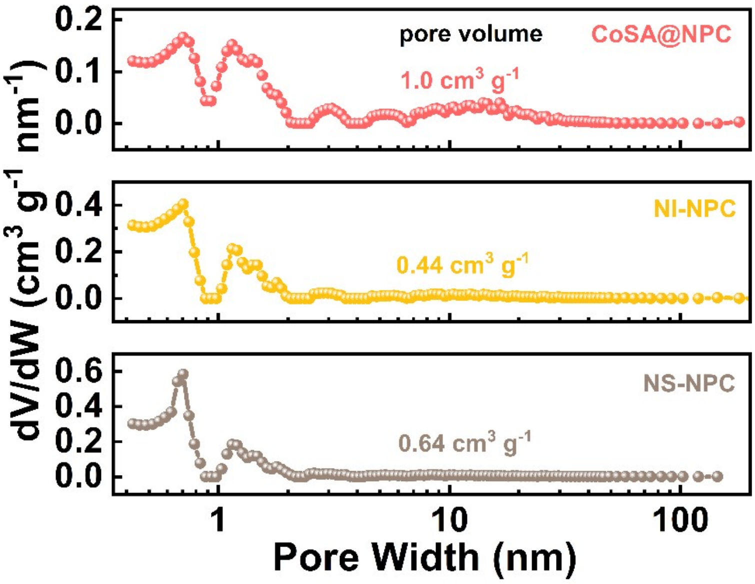

Fig. S8 Pore size distribution of CoSA@NPC, NI-NPC and NS-NPC.

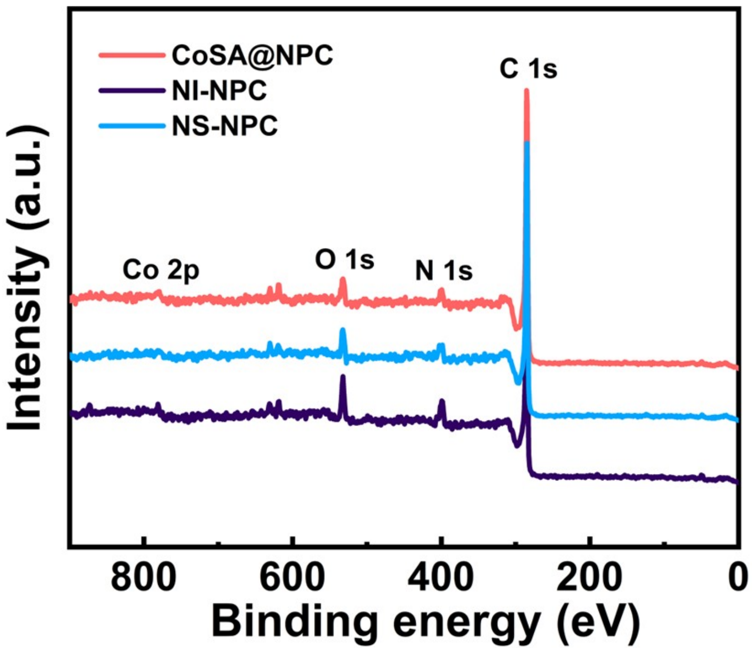

Fig. S9 XPS spectra of CoSA@NPC, NI-NPC and NS-NPC.

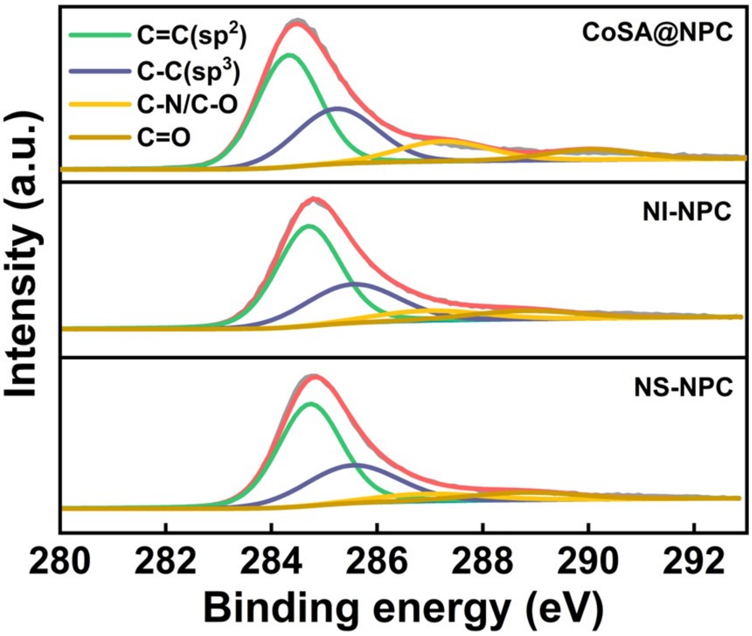

Fig. S10 The high-resolution C 1s XPS spectra of CoSA@NPC, NI-NPC and NS-NPC.

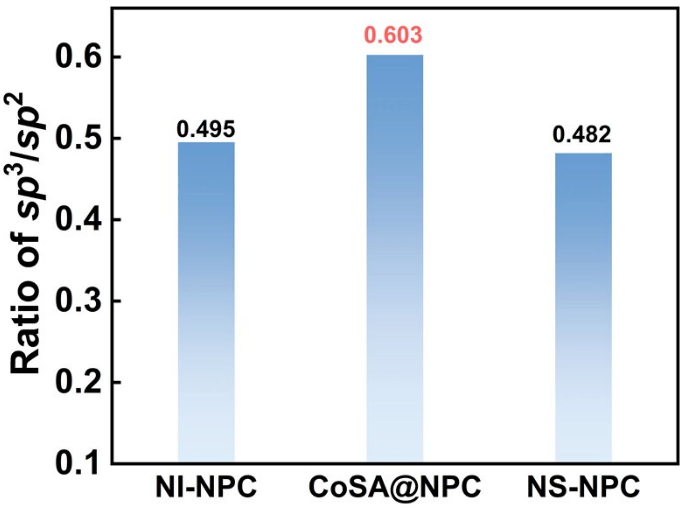

Fig. S11 Ratios of sp^3 C and sp^2 C (sp^3 /sp^2) of NI-NPC, CoSA@NPC, NS-NPC.

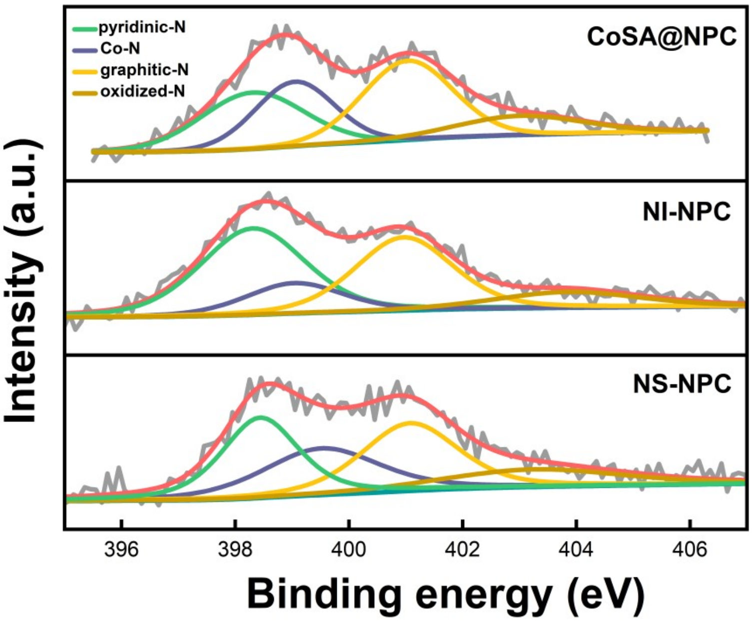

Fig. S12 The high-resolution N 1s XPS spectra of CoSA@NPC, NI-NPC and NS-NPC.

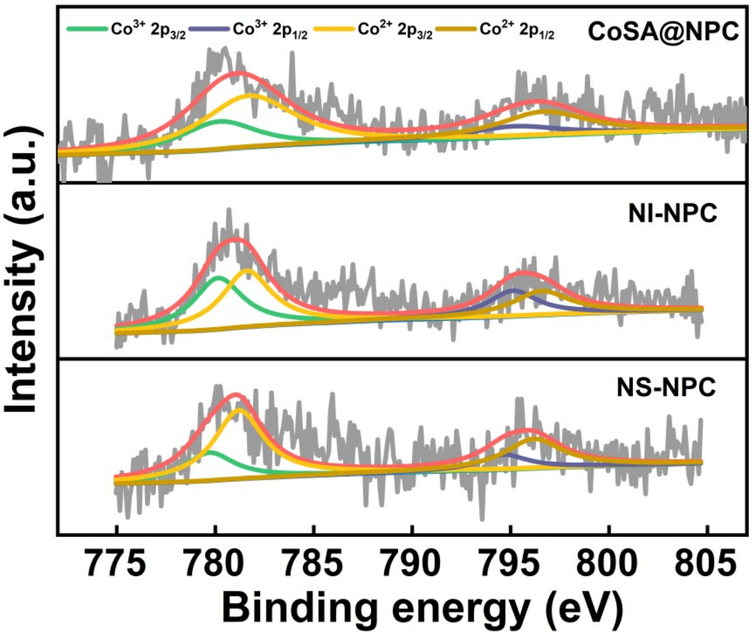

Fig. S13 The high-resolution Co 2p XPS spectra of CoSA@NPC, NI-NPC and NS-NPC.

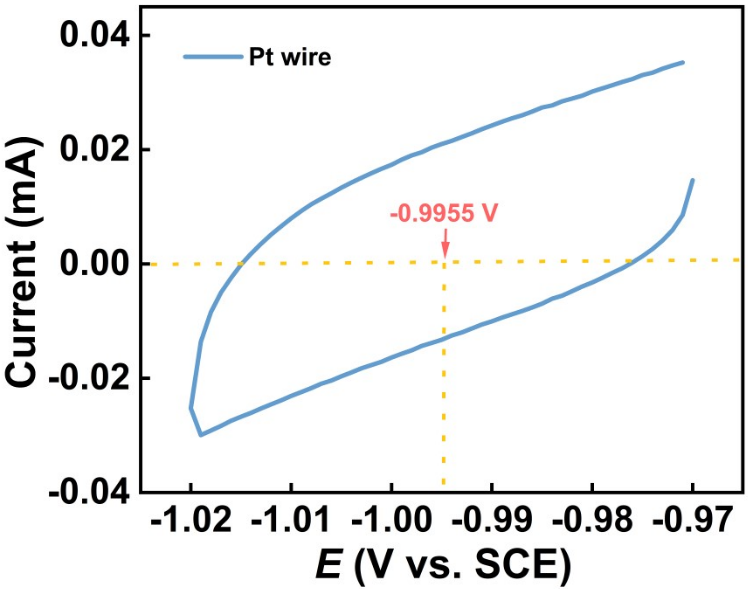

Fig. S14 The calibration result of saturated calomel electrode (SCE) reference electrode to RHE in H_2-saturated 0.1 M KOH.

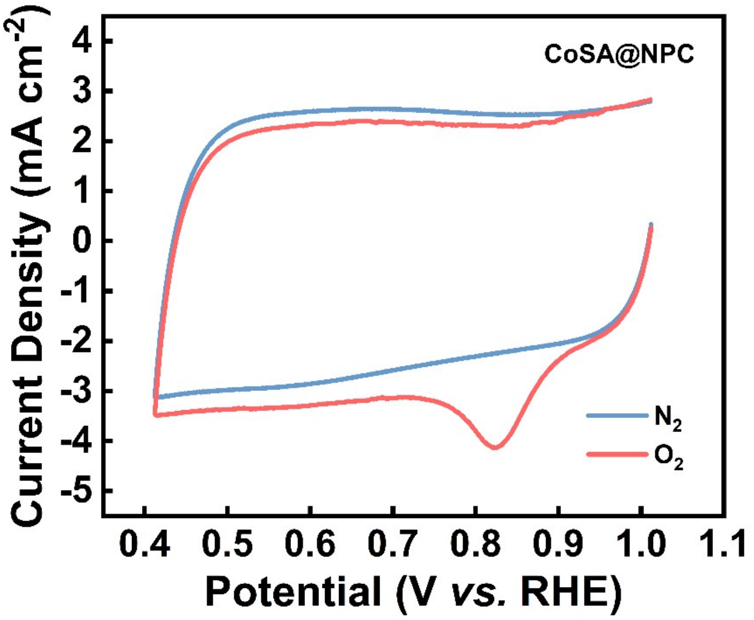

Fig. S15 Cyclic voltammograms of CoSA@NPC in N_2 or O_2-saturated 0.1 M KOH.

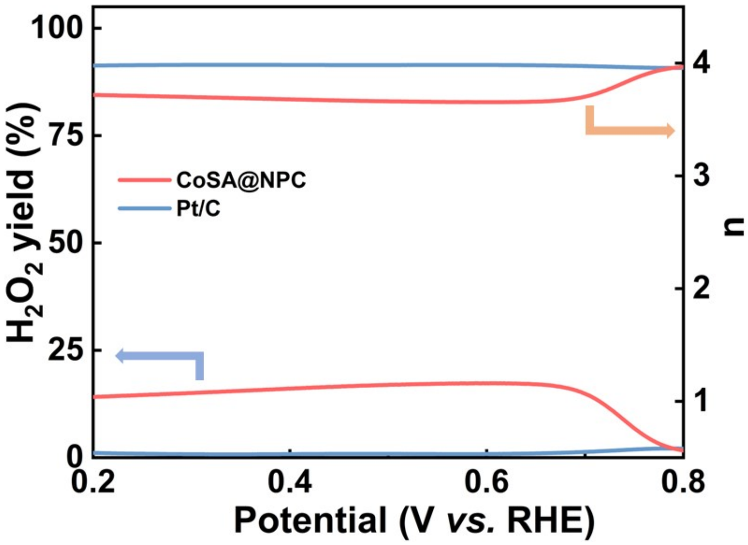

Fig. S16 Electron transfer number and H_2O_2 yield of CoSA@NPC and Commercial Pt/C.

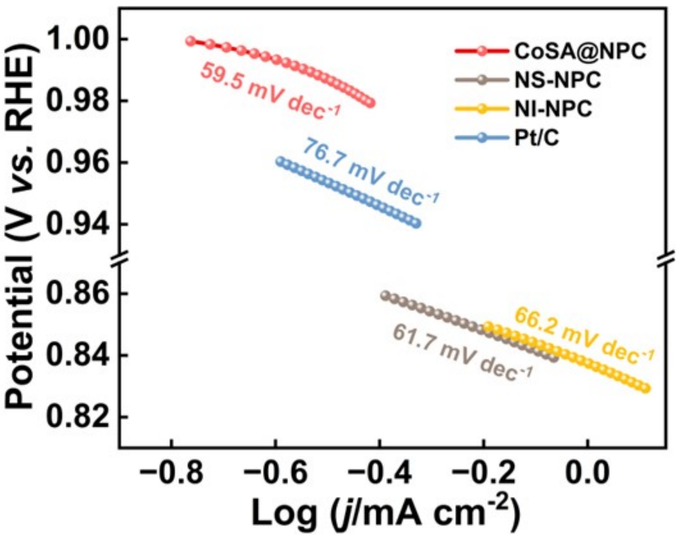

Fig. S17 Tafel plots of ORR calaculated from LSV curves.

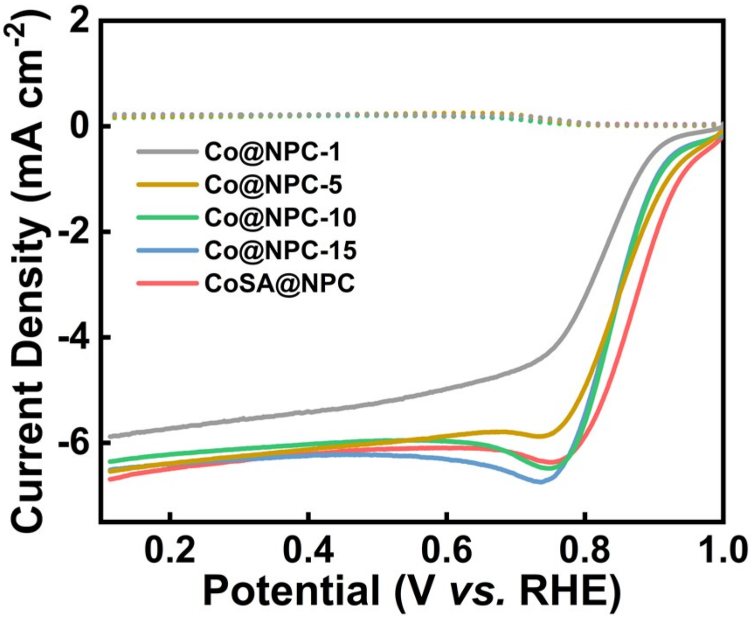

Fig. S18 LSV polarization curves of Co@NPC-x (x=1, 5, 10, 15) and CoSA@NPC for ORR in 0.1 M KOH.

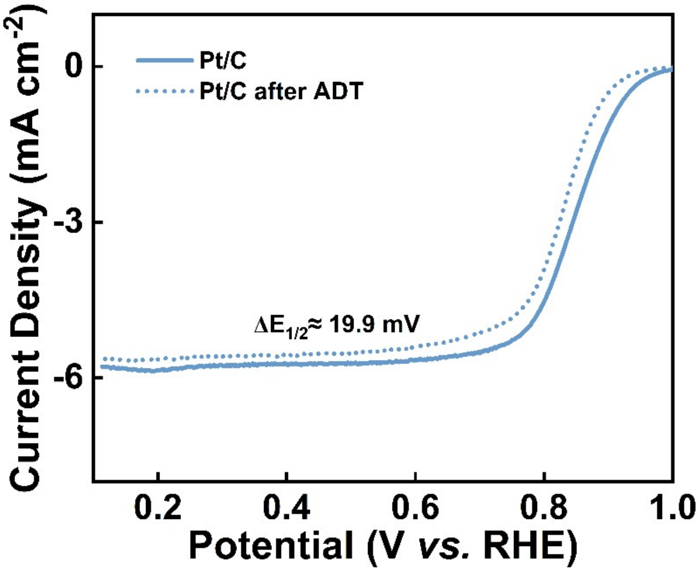

Fig. S19 LSV of Pt/C before and after 5000 CV cycles in 0.1 M KOH.

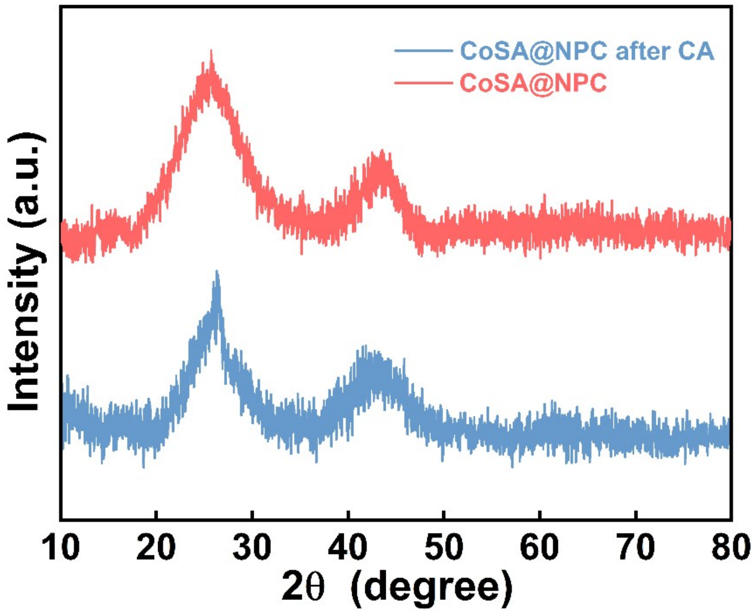

Fig. S20 XRD patterns of CoSA@NPC before and after the CA test.

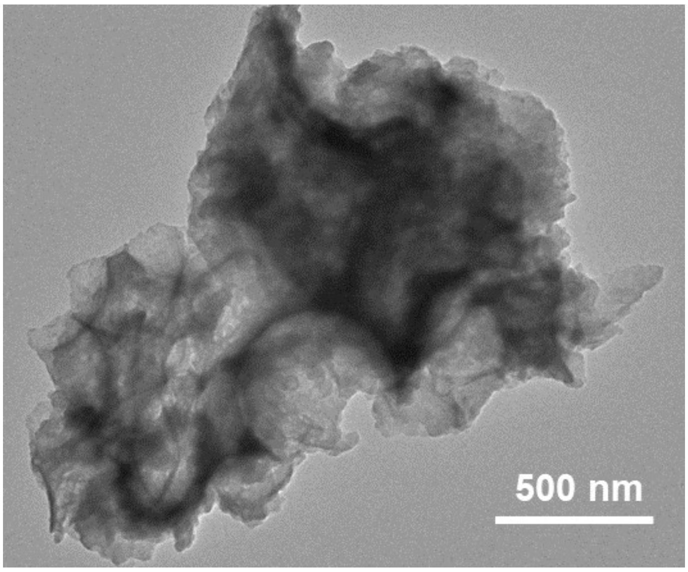

Fig. S21 TEM image of the CoSA@NPC after stability test.

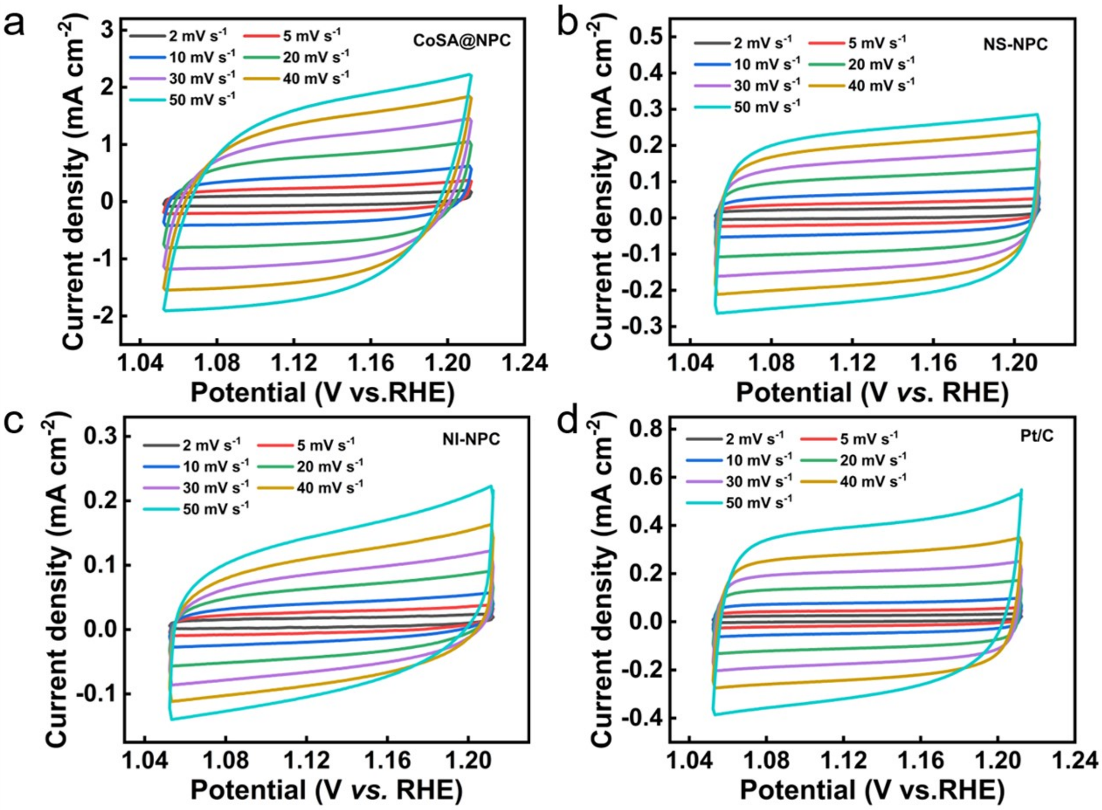

Fig. S22 CV curves of (a) CoSA@NPC (b) NS-NPC (c) NI-NPC and (d) Pt/C in the double-layer region at scan rates of 2, 5, 10, 20, 30, 40 and 50 mV s^{-1} in 0.1 M KOH.

Fig. S23 The photo of open-circuit voltage measurement (with a multimeter) for CoSA@NPC-based ZAB**.**

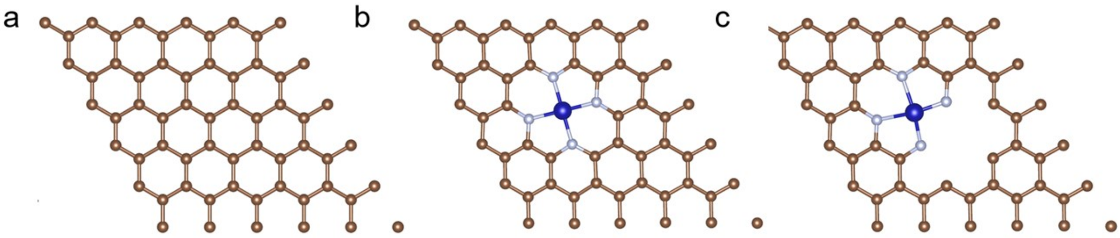

Fig. S24 The optimized models of (a) pure C (b) pure C-Co-N_4 (c) defect C-Co-N_4.

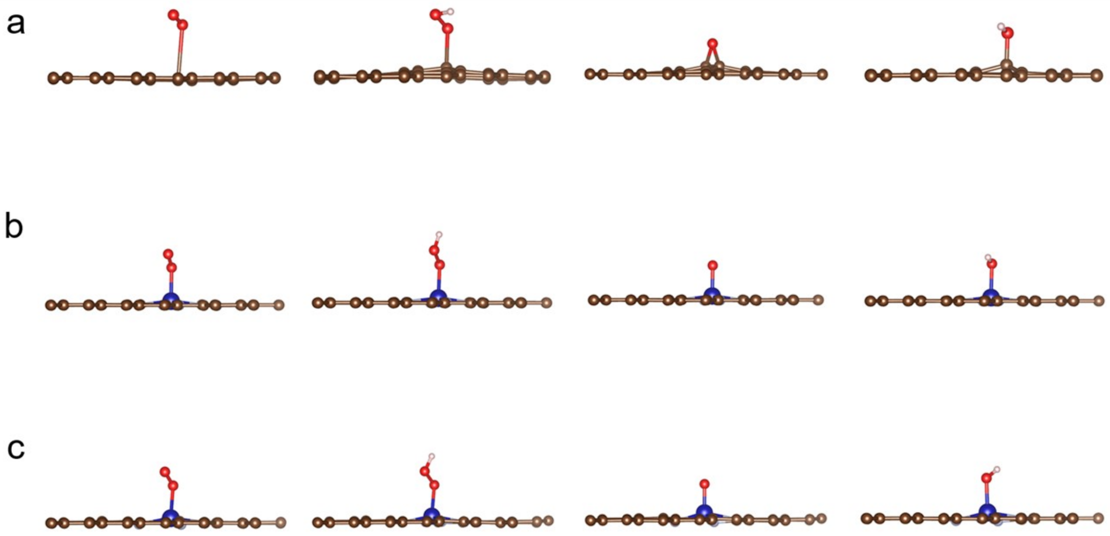

Fig. S25 Oxygen intermediates in ORR process (O_2, OOH*, O*, and OH*) adsorbed on (a) pure C, (b) pure C-Co-N_4, (c) defect C-Co-N_4 models, respectively.

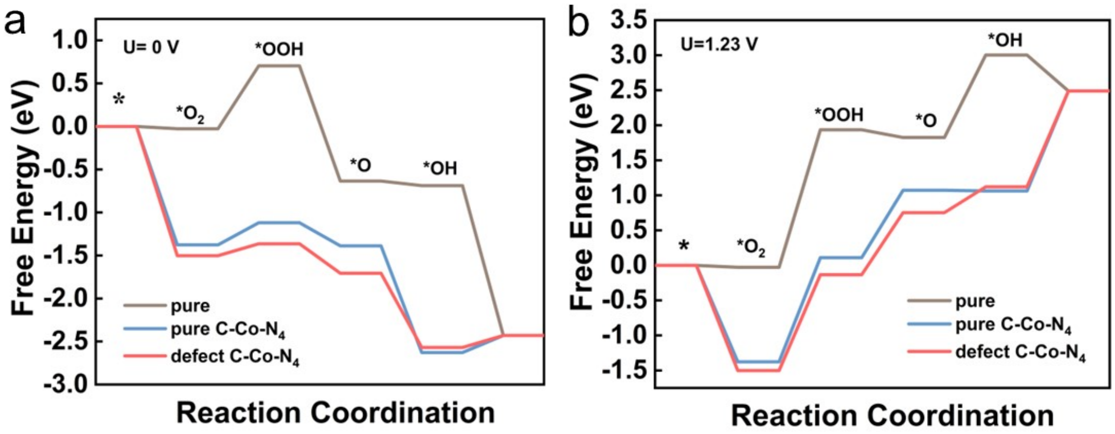

Fig. S26 The calculated energy profile for ORR on different sites with (a) U= 0 V, (b) 1.23 V.

Table S1 Co contents in the obtained samples determined by ICP-OES.

Samples	Co (wt.%)
NI-NPC	1.96
NS-NPC	2.43
CoSA@NPC	2.88

Table S2 The porosity of as-prepared catalysts

Samples	BET surface area (m^2 g^{-1})	Pore volume (cm^3 g^{-1})
CoSA@NPC	851.2	1.0
NI-NPC	636.9	0.44
NS-NPC	635.2	0.64

Table S3 The content of C=C(sp^2), C-C(sp^3), C-N/C-O, and C=O in different catalysts

Samples	C=C (%)	C-C (%)	C-N/C-O (%)	C=O (%)	sp^3/sp^2
CoSA@NPC	50.14	30.21	12.93	6.71	0.603
NI-NPC	56.68	28.07	7.56	7.68	0.495
NS-NPC	59	28.42	6.37	6.2	0.482

Table S4 The content of Pyridinic-N, Co-N, Graphitic-N, and Oxidized-N in different catalysts.

Samples	Pyridinic-N (%)	Co-N (%)	Graphitic-N (%)	Oxidized-N (%)
CoSA@NPC	28.16	21.13	34.59	16.12
NI-NPC	33.11	28.79	27.92	10.18
NS-NPC	28.78	34.73	21.82	14.67

Table S5 EXAFS fitting parameters of CoSA@NPC for various models.

Models	Shell	*N*[a]	R (Å)[b]	σ^2 (Å^2)[c]	ΔE_0 (eV)[d]	R factor[e]
Co-N_4	Co-N	4.8±0.66	1.885±0.0071	0.0057± 0.00159	6.462±1.988	0.004
Co-N_3C	Co-N	6.0±0.64	1.885±0.0085	0.0064±0.00325	10.446±3.464	0.017
	Co-C	0.668±0.21	1.885±0.219	0.0020±0.00547		
Co-N_2C_2	Co-N	3.67±0.50	1.885± 0.121	0.016± 0.011	4.032±2.748	0.016
	Co-C	3.67±0.50	1.885±0.0324	0.0025±0.00174		
Co-N_3O	Co-N	2.69±0.72	1.885±0.0559	0.0021±0.00787	1.813±3.502	0.011
	Co-O	0.90±0.24	1.885±0.0713	0.00081± 0.00835		

Note: Note: [a] N: coordination numbers; [b] R: bond distance; [c] σ^2: Debye–Waller factors; [d] ΔE_0: the inner potential correction; [e] R factor: goodness of fit. Among all the fittings models, Co-N_4 exhibited the best fitting result (Table S5). Moreover, the EXAFS fitting demonstrates an average bonding mode, and cannot completely rule out the possibilities for the existence of other chemical bonds.

Table S6 ORR performance in 0.1 M KOH of all catalysts.

Samples	$E_{1/2}$ (V)	E_{onset} (V)	Tafel (mV dec^{-1})	j_k (mA cm^{-2})	j_m (mA mg^{-1})	TOF (e s^{-1} $site^{-1}$)	C_{dl} (mF cm^{-2})
CoSA@NPC	**0.878**	**0.99**	**59.5**	**12.39**	**1076**	**0.66**	**66.7**
NI-NPC	0.805	0.872	66.2	0.73	93	0.06	4.8
NS-NPC	0.8	0.865	61.7	0.68	70	0.04	9.3
Pt/C	0.85	0.95	76.7	5.65	236	0.48	13.8

Table S7 Comparison of ORR performances of CoSA@NPC in 0.1 M KOH with other reported Cobalt-based catalysts.

Samples	$E_{1/2}$ (V)	E_{onset} (V)	Reference
CoSA@NPC	**0.878**	**0.99**	**This work**
CoSA /N, S-HCS	0.85	0.96	[3]
Co@DMOF-900	0.86	0.94	[4]
Co/N CCPC-3	0.827	0.921	[5]
Co/$ZnCo_2O_4$@NC-CNTs	0.9	1.01	[6]
Mo_2C/Co@NC	0.86	0.95	[7]
SS-Co-SAC NSAs	0.81	-	[8]
Co-SAs/SNPs@NC	0.898	1.03	[9]
Co@IC/MoC@PC	0.875	1.034	[10]
Co/N@CNTs@CNMF-800	0.86	0.99	[11]
Co-POC	0.83	-	[12]
Co/PC	0.92	1	[13]
CoSA + Co_9S_8/HCNT	0.855	0.92	[14]
Co SA@NCF/CNF	0.88	-	[15]

Table S8 Comparison of ZAB performance of CoSA@NPC with other reported Cobalt-based catalysts.

Catalysts	OCV (V)	Specific capacity (mAh g^{-1})	Stability (h)	Maximum power density (mW cm^{-2})	Reference
CoSA@NPC	**1.44**	**905**	**350**	**153.6**	**this work**
Co@DMOF-900	1.45	815	200	158	[4]
CoSA/N, S-HCS	1.5	846.7	166.7	173.1	[16]
Co-SAs@NC	1.46	897.1	~15	105.3	[17]
SS-Co-SAC NSAs	1.52	714.2	-	195.1	[8]
$Fe_{0.5}$Co@HOMNCP	1.619	768.5	120	134	[18]
CoSA + Co_9S_8/HCNT	1.412	~800	24	177.33	[14]
Mo_2C/Co@NC	1.41	691	180	187.9	[7]
Co/N CCPC-3	1.48	707	40	87	[5]
Co@IC/MoC@PC	1.482	728	90	221.4	[10]
CoO/N-CNT+ NiFe LDH	-	-	200	~265	[19]
Co@NCNTA-700	-	770	170	-	[20]
Pd@3DOM-Co_3O_4	-	-	50	-	[21]

References

[1] W. Li, D. Zhao, *Adv. Mater.,* 2013, **25(37)***,* 5129-5152.

[2] J. K. Nørskov, J. Rossmeisl, A. Logadottir, L. Lindqvist, J. R. Kitchin, T. Bligaard, H. Jonsson, *J. Phys. Chem. B.,* 2004, **108,** 17886-17892.

[3] Z. Zhang, X. Zhao, S. Xi, L. Zhang, Z. Chen, Z. Zeng, M. Huang, H. Yang, B. Liu, S. J. Pennycook, *Adv. Energy. Mater.,* 2020, **10,** 2002896.

[4] S. Yuan, J. Zhang, L. Hu, J. Li, S. Li, Y. Gao, Q. Zhang, L. Gu, W. Yang, X. Feng, *Angew. Chem., Int. Ed.,* 2021, **133,** 21853-21858.

[5] T. Wang, Y. He, Y. Liu, F. Guo, X. Li, H. Chen, H. Li, Z. Lin, *Nano Energy.,* 2021, **79**, 105487.

[6] L. Yan, Z. Xu, W. Hu, J. Ning, Y. Zhong, Y. Hu, *Nano Energy.,* 2021, **82,** 105710.

[7] T. Gu, R. Sa, L. Zhang, D.-S. Li, R. Wang, *Appl. Catal., B,* 2021, **296,** 120360.

[8] W. Xie, Y. Song, S. Li, J. Li, Y. Yang, W. Liu, M. Shao, M. Wei, *Adv. Funct. Mater.,* 2019, **29,** 1906477.

[9] Z. Wang, C. Zhu, H. Tan, J. Liu, L. Xu, Y. Zhang, Y. Liu, X. Zou, Z. Liu, X. Lu, *Adv. Funct. Mater.,* 2021, **31,** 2104735.

[10] L. Zhang, Y. Zhu, Z. Nie, Z. Li, Y. Ye, L. Li, J. Hong, Z. Bi, Y. Zhou, G. Hu, *ACS Nano.* 2021, **15,** 13399-13414.

[11] T. Liu, J. Mou, Z. Wu, C. Lv, J. Huang, M. Liu, *Adv. Funct. Mater.,* 2020, **30,** 2003407.

[12] B. Q. Li, C. X. Zhao, S. Chen, J. N. Liu, X. Chen, L. Song, Q. Zhang, *Adv. Mater.,* 2019, **31,** 1900592.

[13] T. Zhou, H. Shan, H. Yu, C. a. Zhong, J. Ge, N. Zhang, W. Chu, W. Yan, Q. Xu, H. a. Wu, *Adv. Mater.,* 2020, **32,** 2003251.

[14] Y. Li, R. Cao, L. Li, X. Tang, T. Chu, B. Huang, K. Yuan, Y. Chen, *Small.,* 2020, **16,** 1906735.

[15] D. Ji, L. Fan, L. Li, S. Peng, D. Yu, J. Song, S. Ramakrishna, S. Guo, *Adv. Mater.,* 2019, **31,** 1808267.

[16] Z. Zhang, X. Zhao, S. Xi, L. Zhang, Z. Chen, Z. Zeng, M. Huang, H. Yang, B. Liu, S. J. Pennycook, *Adv. Energy. Mater.,* 2020, **10,** 2070195.

[17] X. Han, X. Ling, Y. Wang, T. Ma, C. Zhong, W. Hu, Y. Deng, *Angew. Chem., Int. Ed.,* 2019, **131,** 5413-5418.

[18] W. Li, B. Liu, D. Liu, P. Guo, J. Liu, R. Wang, Y. Guo, X. Tu, H. Pan, D. Sun, *Adv. Mater.,* 2022, 2109605.

[19] B. J. Hopkins, C. N. Chervin, J. W. Long, D. R. Rolison, J. F. Parker, *ACS Energy Lett*., 2020, **5**, 3405-3408.

[20] L. Liu, Y. Wang, F. Yan, C. Zhu, B. Geng, Y. Chen, S. l. Chou, *Small. Methods*, 2020, **4**, 1900571.

[21] J. Fu, R. Liang, G. Liu, A. Yu, Z. Bai, L. Yang, Z. Chen, *Adv. Mater*., 2019, **31**, 1805230.

Author Contributions

X.F., B.W. and W.Y. directed the research and revised the manuscript. L.L. executed the experiments, analyzed the data, and wrote the initial manuscript. J. W. and Y. L. built the test system of ORR. R. L. conducted SEM measurement. X. L and C. W. drawn the diagram of catalyst preparation.